

# TUTDoR

## On the effect of deformation conditions on the metal flow behavior during upsetting process using finite element simulation DEFORM 3D software.

Item Type	Article
Authors	Obiko, Japheth;Shongwe, Mxolisi Brendon;Malatji, Nicholus
DOI	<a href="https://doi.org/10.1007/s12008-024-02051-2">https://doi.org/10.1007/s12008-024-02051-2</a>
Publisher	Springer
Rights	Attribution-NonCommercial-ShareAlike 4.0 International
Download date	2026-06-11 00:14:29
Item License	<a href="http://creativecommons.org/licenses/by-nc-sa/4.0/">http://creativecommons.org/licenses/by-nc-sa/4.0/</a>
Link to Item	<a href="https://hdl.handle.net/20.500.14519/1536">https://hdl.handle.net/20.500.14519/1536</a>



# On the effect of deformation conditions on the metal flow behavior during upsetting process using finite element simulation DEFORM 3D software

Japheth Obiko<sup>1</sup> · Mxolisi Brendon Shongwe<sup>1</sup> · Nicholus Malatji<sup>1</sup>

Received: 12 April 2024 / Accepted: 29 July 2024  
© The Author(s) 2024

## Abstract

The study reports on the metal flow behaviour during upsetting or forging using the finite element method. Forging simulation studied the metal flow behaviour of a laboratory-sized specimen and a cylindrical engine connecting rod specimen of AISI 52100 high-chromium steel specified in the software database. The focus was to study the effect of deformation conditions (temperature and die velocity) on metal flow behaviour during forging. The simulation results showed heterogeneous metal flow behaviour during forging. Hence, this indicates that effective flow stress and flow strain, particle flow velocity, effective strain rate, damage and temperature distribution exhibited inhomogeneous deformation behaviour. As the temperature increased, the forging load decreased, thus a decrease in deformation resistance. The simulation of the engine connecting rod further confirmed inhomogeneous deformation during forging. Damage coefficient results show that the crack pin end had a higher damage probability during forging. This study clearly showed that finite element simulation can predict metal flow behaviour during the forging of AISI 52100 steel. The study output provides a basis for analysing and optimising most industrial metal forming processes using a numerical simulation approach. Hence, this method is effective in predicting flow behaviour.

**Keywords** Deform 3D · Finite element simulation · Deformation behaviour · Flow stress and strain · AISI 52100 steel

## 1 Introduction

The processing route of industrial structural and functional components is achieved through metal-forming processes such as forging, rolling, extrusion and wire drawing [1, 2]. For example, forging is the manufacturing technique for industrial machine parts such as gears and crankshafts [3]. During forging, metallic materials undergo severe plastic deformation and stress [4, 5]. Large plastic deformation induces microstructural changes in the material, hence affecting the mechanical properties of the material [6]. The grain refinement occurs due to severe plastic deformation during forging [7]. The metal flow behaviour plays a role in shaping the final product quality [8]. High-end research in metal forming has been a topic of concern to predict the flow behaviour of metal and alloys during forging [9–12]. The study of flow

characteristics of metals under severe deformation is to determine the load requirements during forming [13]. The flow stress–strain curves assist in predicting the forming parameters. Metal forming parameters such as strain hardening can be easily derived from the developed constitutive equations [14]. The forming parameters, therefore, provide the basis for the design of dies and other machine components for the forging machine [15]. To this end, understanding the metal flow behaviour is paramount in designing forming tools and components.

Due to large deformation forces and stresses experienced during forging, metal flow analysis is complex [4, 5]. The metal flow analysis poses a challenge due to heat generated by frictional forces, which affect the flow stress behaviour [6, 16]. The internal heat generated directly affects the flow behaviour [17], hence the product quality. During forging, material flow properties are temperature and strain-rate sensitive, thus affecting metal flow behaviour. The increase in temperature due to interfacial friction invalidates flow stress measurements [16]. Therefore, final product quality depends on the lubricant quality, which reduces interfacial friction, thus reducing the barrelling effect resulting

---

✉ Japheth Obiko  
japheth.obiko97@gmail.com

<sup>1</sup> Tshwane University of Technology-Pretoria, Pretoria, South Africa

in a homogeneous deformation [18, 19]. Evans and Scanning [17] suggested the analytical equations for correcting flow stress with friction effect. Several other researchers have adopted the same equations to correct flow stress after forging [20–23]. The flow stress correction applies only to laboratory-tested samples after thermomechanical processing using equipment such as the Gleeble thermal mechanical simulator. Therefore, there is a need for more industrial-based studies to provide insights into metal flow behaviour at higher strain and strain rates. Hence, industries should integrate a high-computing simulation module into their production process for process parameter optimisation. This approach will reduce production costs and improve efficiency.

From the industrial perspective, the production of quality products depends on the experience of engineers and the trial and error method [2, 24], hence high production costs and time-consuming [8, 24]. As a result, new analysis techniques, such as the finite element methods, are used widely to study metal flow behaviour [25–28]. These techniques reduce the cost of production by optimising the production process [24]. Computer software tools such as Deform 3D, ANSYS and Abaqus find application in studying and optimising the forging process of metal and alloys [13, 24]. However, the accuracy of finite element simulation depends on the constitutive equations developed using experimental data [29]. The constitutive equations are the most common method of studying the hot deformation behaviour in metal and alloys. These equations model the relationship between the flow stress and the deformation conditions such as temperature, strain and strain rate during forming. These equations provide information on the flow stress characteristics and act as input codes for the computational simulation of metal forming [11, 30–34]. The constitutive models commonly used in metal forming analysis include:

- Phenomenological model: This model considers the continuum mechanics and thermodynamic irreversibility. During analysis, the model accounts for the deformation mechanisms, such as work hardening due to dislocation and dynamic softening (recrystallisation and recovery) that occur during forming ascribed to thermal activation.
- Artificial neural network models: This model has been recently used to solve complex metal forming problems, which poses a challenge when solving using constitutive equations.
- Physical-based model: This model mainly considers dislocation density theory and dynamic recrystallisation kinetics during forming.

The basis of classifications of these equations is mainly on the computational parameters used to quantify the flow stress behaviour pattern during forming [35]. Physical models are

complex compared to phenomenological models. The phenomenological model, especially the Arrhenius constitutive, is commonly used to describe the relationship between flow stress, temperature, strain and strain rate [8–13]. Researchers have used the Arrhenius type model to characterise the flow stress behaviour of metal and alloys such as aluminium alloys [18–20], 35CrMo steel [17], P92 steel [7, 12, 13], 9Cr-1Mo steel [31], 20CrMo alloy steel [36], Nickel-based superalloy [37], magnesium alloys [22] and titanium alloys [38]. The developed equations predict the flow stress behaviour. This equation acts as input code for numerical simulation.

The current study focuses on how finite element simulation can be applied in studying the influence of deformation parameters on the metal flow behaviour during forming. This study provides the required information for process and tool designers to understand fully the metal flow pattern during the metal forming process. In this study, to demonstrate the metal flow behaviour during forming, AISI 52100 steel was used. This steel finds application in manufacturing mechanical components such as pipes, tubes, extrusion tools and bearings. The wide application of this steel is due to its high wear resistance and contact fatigue. During production, the processing route involves melting, casting and then forging or hot rolling before heat treatment. Hence, this steel is suitable for this study to illustrate the effect of deformation conditions on metal flow behaviour.

## 2 Finite element simulation theory

Finite element method (FEM) software can analyse and optimise the forging (upsetting) process [39]. The modelling of this process is based on rigid-viscoelasticity using the variational principle [40]. This model assumes that: (a) Elastic strain is negligible compared to plastic strain. Hence, the analysis ignored the elastic strain during the analysis (b) The volume of the workpiece is incompressible (c) The workpiece exhibits isotropic characteristics. The theory behind FEM has been widely discussed elsewhere in the literature [40–42]. The highlight of the FEM simulation theory is in this section. In this method, the analysis approach uses functional variation minimisation to study stress and strain fields (Eq. 1).

$$\delta\varphi = \int_v \sigma_i \delta\dot{\epsilon}_i dv + \int_v K \dot{\epsilon}_v \delta\dot{\epsilon}_v dv - \int_{SF} F_i \delta u_i ds = 0 \quad (1)$$

where,

$$\sigma_i = \sqrt{3/2} \left( \begin{matrix} \sigma' & \sigma' \\ \sigma' & \sigma' \end{matrix} \right)^{1/2}, \quad \dot{\epsilon} = \sqrt{2/3} (\dot{\epsilon}_{ij} \dot{\epsilon}_{ij})^{1/2} \quad (2)$$

In Eq. 2,  $\sigma_i$  is the effective stress,  $\varepsilon_i$  is the effective strain respectively,  $u_i$  is the surface velocity components,  $SF$  denotes the surface force,  $S_v$  is the surface velocity,  $F_i$  is the traction stress,  $\dot{\varepsilon}_v$  is the volumetric strain rate,  $v$  is the volume of the billet and  $K$  is the penalty constant for volume change [41],  $\sigma'_{ij}$  is the deviatoric stress tensor and  $\dot{\varepsilon}_{ij}$  is the strain rate tensor [40].

During the isothermal forging process, the deformation temperature within the billet is kept constant. However, in industrial practice, the isothermal process is unattainable. During deformation, internal heat generation causes temperature variation. During forging, the temperature field can be calculated by FEM simulation using the Fourier formulation [41] as in Eq. 3.

$$\nabla^T(K\nabla T) + \dot{q} - \rho C_p \delta T / \delta t = 0 \quad (3)$$

In Eq. 3,  $K$  is the thermal conductivity,  $T$  is the temperature in Kelvin (K),  $\dot{q}$  is the heat generation rate during plastic deformation,  $\rho$  is the material-specific density,  $C_p$  is the specific heat capacity and  $t$  is time (sec) (Eq. 3). The rate of heat generation during the plastic deformation stage is given in Eq. 4.

$$Q(T) = \alpha \sigma_i \dot{\varepsilon}_i \quad (4)$$

where  $\alpha$  is the fraction of mechanical energy converted to heat during deformation, assumed to be 0.9 [17, 40, 43].

The temperature distribution between the die and the workpiece can be determined by solving the energy equation using the weighted residual method [40], as follows Eq. 5:

$$\int_v k T_{,i} \delta T_{,i} dV + \int_v \rho c_p \dot{T} \delta T dV - \int_v \alpha \sigma_i \dot{\varepsilon}_i \delta T dV = \int_s q_n \delta T ds \quad (5)$$

In a FEM simulation, the effect of interfacial friction between the die-workpiece is taken to be of shear type [41]. This friction plays an important role during forging. The friction produces a shear force that restricts metal flow in the die [44]. Thus, the frictional shear stress  $\tau_f$  is expressed as shown in Eq. 6 [42].

$$\tau_f = -mk \left[ \frac{2}{\pi} \tan^{-1} \left( \frac{\vec{v}_s}{\mu_0} \right) \right] t \quad (6)$$

In Eq. 6,  $m$  is the coefficient of friction calculated using the deformed sample geometry ( $0 \leq m \leq 1$ ),  $\vec{v}_s$  is the velocity vector of the workpiece to the anvil,  $k$  is the local flow stress due to shear,  $\mu_0$  is a constant ( $\mu_0 \ll \vec{v}_s$ ) and  $t$  is the unit vector.

### 3 Finite element modelling

Finite element analysis (FEA) is a digital tool widely used to solve real-life problems in the manufacturing industry, particularly in shaping technology. FEA simulation codes can approximate metal flow behaviour and process parameter optimisation. The use of computer codes for industrial processes reduces production costs and time. In this study, FEA analysis evaluates the metal flow behaviour during upsetting (forging). AISI 52100 high chromium bearing steel was used as the workpiece material to study the metal flow behaviour. AISI 52100 steel finds application in the manufacturing industry due to its superior properties, such as high wear and corrosion resistance, flexural strength and desirable dimensional stability [33]. This steel manufactures industrial components such as bearing rings, ball screws and other mechanical components through forging [33, 45].

Forging, particularly upsetting, has been widely used to study metal flow behaviour for most metals and alloys by many experts in this study field. Therefore, the study adapted this process to illustrate the effect of loading conditions on metal flow behaviour. The finite element simulation model was designed using the primitive geometry built-in Deform® 3D software. For the upsetting model, the cylinder (workpiece) and platens (dies) are shown in Fig. 1a. Figure 1b shows the deformed workpiece indicating the strain distribution after simulation. The workpiece geometry dimensions used for the forging simulation were the same as those commonly used for the Gleeble® 3500 thermo-mechanical laboratory testing specimen, as reported in the literature [5]. Table 1 shows the simulation conditions. The upper and lower dies are rigid bodies. The elastic deformation which occurs during forging is negligible. In FEM simulation, the workpiece had discretised into 26,155 tetrahedron elements and 5792 nodes. The whole workpiece volume had a refined mesh to increase the accuracy of the analysis. The dies and specimen interface had a lubricant to reduce friction during the upsetting simulation [8]. During hot forging, frictional shear stress at the die-workpiece interface occurs. A shear-type friction parameter was 0.3 between the die and the workpiece [28]. An illustration of the effect of deformation conditions is further reported herein by a forging simulation of the connecting rod. Table 2 shows the connecting rod simulation parameters. In the analysis of forging simulation data, the elastic deformation did not influence the data analysis since, during forging, large plastic deformations occur.

### 4 FEM simulation model validation

The accuracy and reliability of the FEM model in predicting metal flow behaviour is of great concern to engineers

**Fig. 1** Finite element model showing meshed workpiece under loading

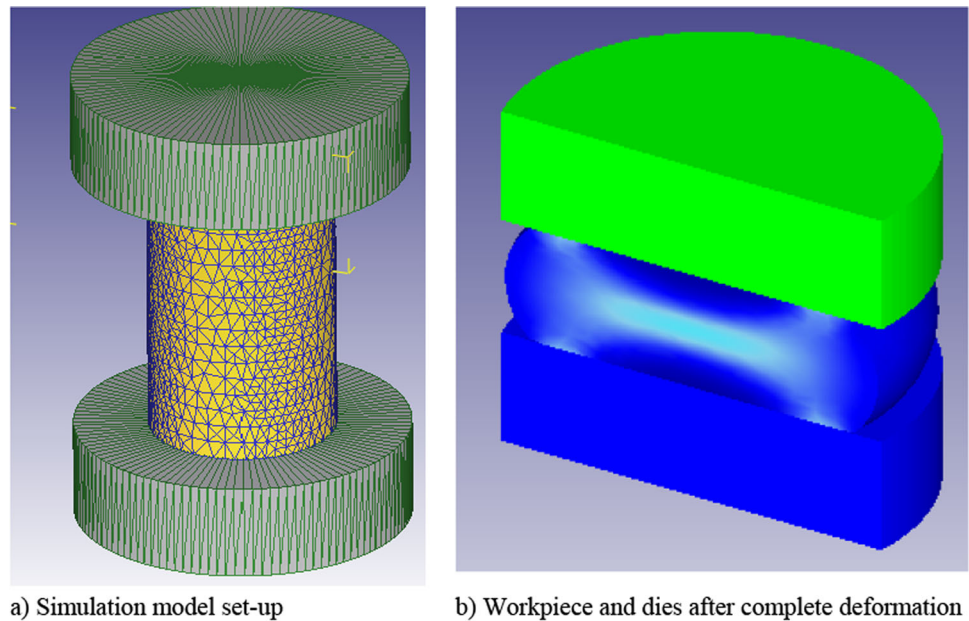


**Table 1** Forging simulation parameters

No	Simulation parameter	Value
1	Workpiece material	AISI 52100 steel
2	Cylinder specimen height (mm)	15
3	Cylinder specimen diameter (mm)	10
4	Forging workpiece temperature (°C)	950, 1050, 1150
5	Upper and lower die temperature (°C)	350
6	Conventional coefficient (N/ (s.mm. °C))	0.02
7	Heat transfer coefficient (N/ (s.mm. °C))	5
8	Number of deformation steps	71
9	Forging environment temperature (°C)	25
10	Upper punch velocity (mm/sec)	5, 10, 50
11	Number of elements	26,155
12	Number of nodes	5792
13	Coefficient of friction (shear-type)	0.3

and designers. The FEM results depend on the constitutive equation, which acts as input codes, mainly obtained from experimental data. Therefore, FEM simulation accuracy depends on an accurate description of material flow behaviour under varying conditions as represented by the constitutive equations.

The following assumptions apply when analysing the forging process using this simulation model: (a) Elastic strain

**Table 2** Connecting rod simulation parameters

Simulation parameters	Description
Workpiece material	AISI 52100
Die material	AISI H13
Mesh element of connecting rod	10,464
Element nodes	2869
Displacement step	0.5
Forging temperature	1150
Die Speed	50
Number of steps	104

\*Other simulation conditions are similar as in Table 1

is negligible compared to plastic strain. Hence, the analysis ignores the elastic strain during the analysis. (b) the volume of the workpiece is incompressible, and (c) the workpiece exhibits isotropic characteristics, as mentioned in Sect. 2. The use of FEM simulation simplifies the real-life physical phenomenon and gives an approximate solution. The obtained solution plays a role during process design and evaluation of the production process. Therefore, the authors strongly assert that the future of any production relies on developed simulation models.

To avoid repetition of model validation, in this study, the developed and validated model used in our previous studies, which is available in the literature [46, 47], was used to investigate the flow stress behaviour as affected by the process parameters.

## 5 Results and discussion

### 5.1 Effect of forging parameters on the forging load

Figure 2 shows the forging load-time flow curves at a given temperature and different die speeds during the forging simulation. The flow curves show that the applied force is proportional to the die speed at a given temperature. The forging load decreases with an increase in the forming temperature (Fig. 2). At a given temperature, the deformation load increases with an increase in die speed and decreases as the forming temperature increases during metal forming [48]. The dependency of flow behaviour on deformation parameters is available in the literature. A study by Zhu et al. [11] showed that the flow stress increases with a decrease in the deformation temperature at a given strain rate. These flow characteristics are sensitive to deformation conditions. At high deformation temperatures, there is a high mobility of atoms, which increases the dislocation driving force. This phenomenon results in lower flow stress [11]. In this study, the forming loads appeared to decrease with an increase in

the die speed at a given forming temperature. This characteristic behaviour is due to the influence of the friction factor during the hot-forming process. At a lower strain rate, high flow stress has been observed to occur due to prolonged die-workpiece contact time, resulting in a change of friction from kinetic to static friction [49]. At a higher die speed, the maximum forming loads decreased (from 42.35 kN, 36.36 kN and 26.34 kN) with an increase in the forming temperature (920 °C, 1050 °C, and 1150 °C), but the loads were lower than those recorded for lower die speeds as shown in Fig. 2.

The variation in the forming loads can be attributed to a higher generation of internal heat, causing softening of the workpiece during forming at higher die speeds. This dynamic softening reduces the forming loads at high die speeds. Evans and Scharning [17] reported that internal heat generation during metal forming reduces the required force to deform the material due to inhomogeneous conditions inside the workpiece. To this end, the actual forming load requires analysis to account for the influence of friction.

Figure 3 shows the load-time curve at a constant die speed at different forming temperatures. The flow curves show that

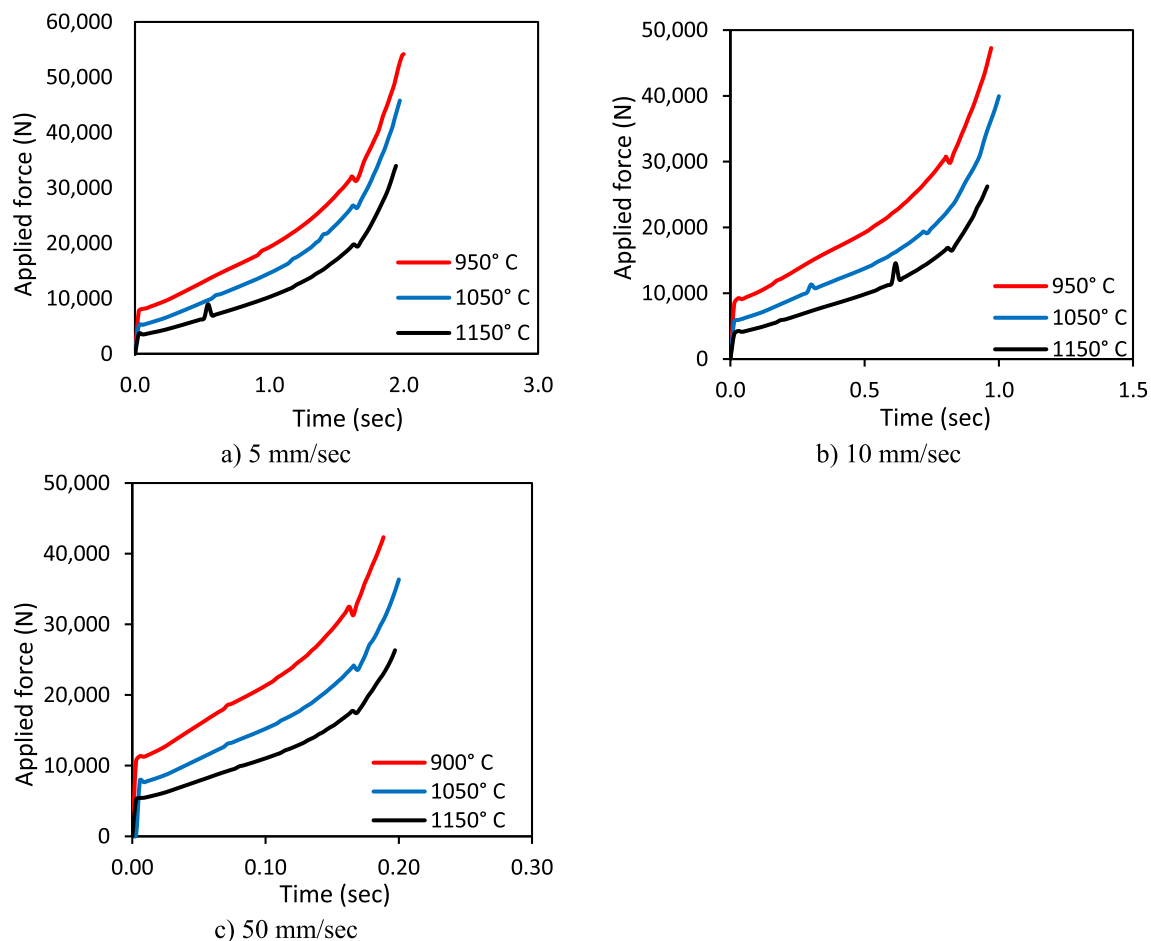
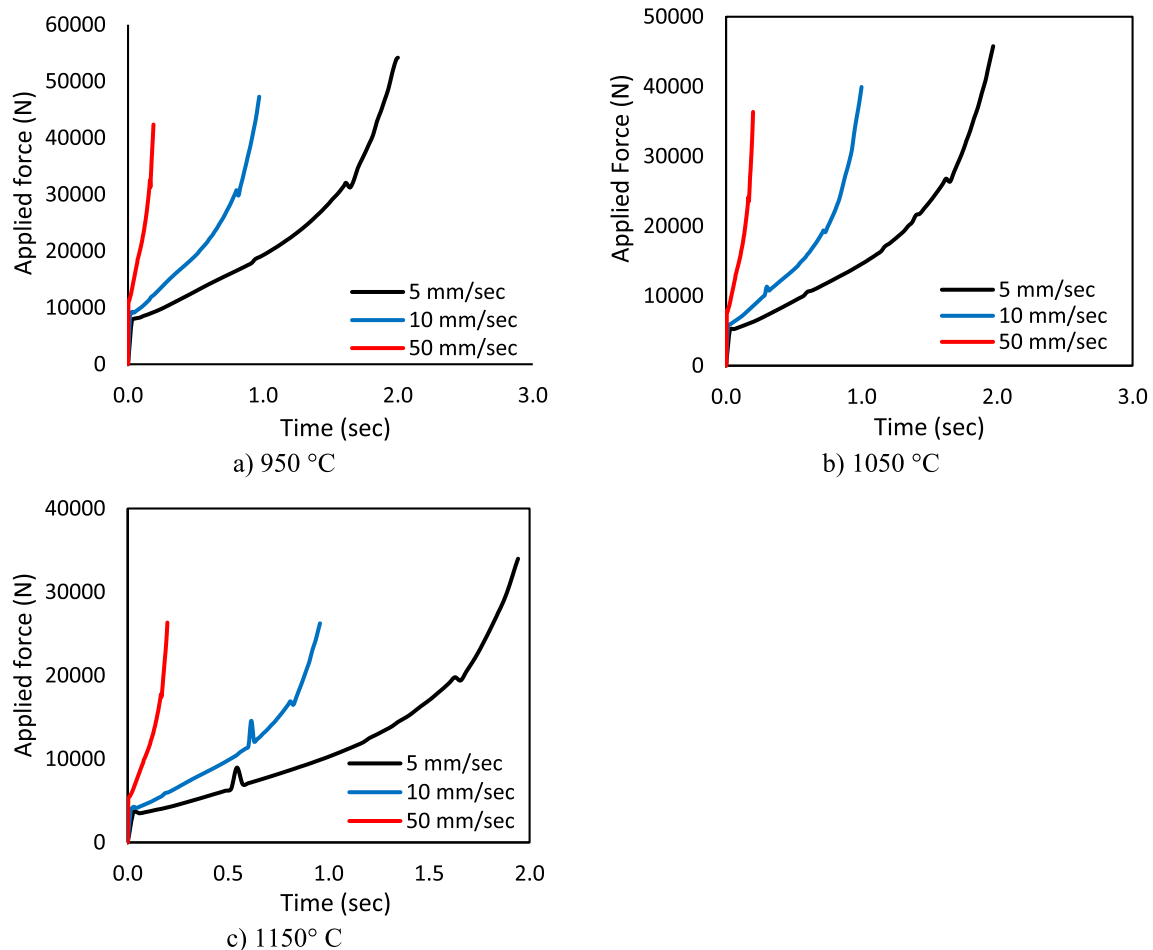


Fig. 2 Load-time curves at a constant die speed and varying forging temperatures



**Fig. 3** Load-time curves at constant forging temperatures and varying die speeds

forging at higher die velocities takes a short time to complete the deformation process as expected compared to lower die velocities. As mentioned earlier, the forging loads are higher at lower die speeds than at higher die speeds. Traditionally, higher flow stress or force is expected to occur at a higher strain rate or die speed than a lower strain rate. Higher velocity causes a generation of internal heat, resulting in temperature rise, thus increasing the mobility of atoms during deformation, lowering the deformation force. From the results, load-time flow curves estimated the forming load. From an industrial perspective, the optimal production process occurs at a low forming load and shorter forming time [48]. In this study, a die velocity of 50 mm/sec and a forming temperature of 1150 °C were the optimal conditions. Therefore, the workability behaviour of AISI52100 steel occurs under these conditions.

## 5.2 Effective strain distribution

The stress and strain distribution provide an avenue to analyse metal flow behaviour during forging. The influence of form-

ing parameters on the metal flow behaviour during forging plays a role in industrial design. Figure 4 shows the strain distribution during forging simulation at a forging temperature of 1150 °C and different die velocities (velocity = 5, 10, and 50 mm/sec). Three points (denoted P1, P2, and P3, Fig. 4), which occur at three different deformation zones during metal forming, the intense shear zone (P1), moderate deformation zone (P2) and the dead-metal zone (P3) [7], provide the basis for this analysis. The three points had strain variation, indicating an inhomogeneous deformation process. The three points used for strain analysis have been categorised by Rasti et al. [7], Point P1 represents the intense shearing zone during forging, hence experiencing severe plastic deformation. Grain refinement occurs in this zone, which can result in dynamic recrystallisation [7, 18]. Point P2 experienced a moderate strain, but this region had a higher effective strain than point P3 and lower than point P1, as shown in Fig. 5. Finally, point P3 represents the dead metal zone. Point P3 experienced a lower effective strain than point P1 and P2, attributed to the shear friction stress at the die-workpiece interface.

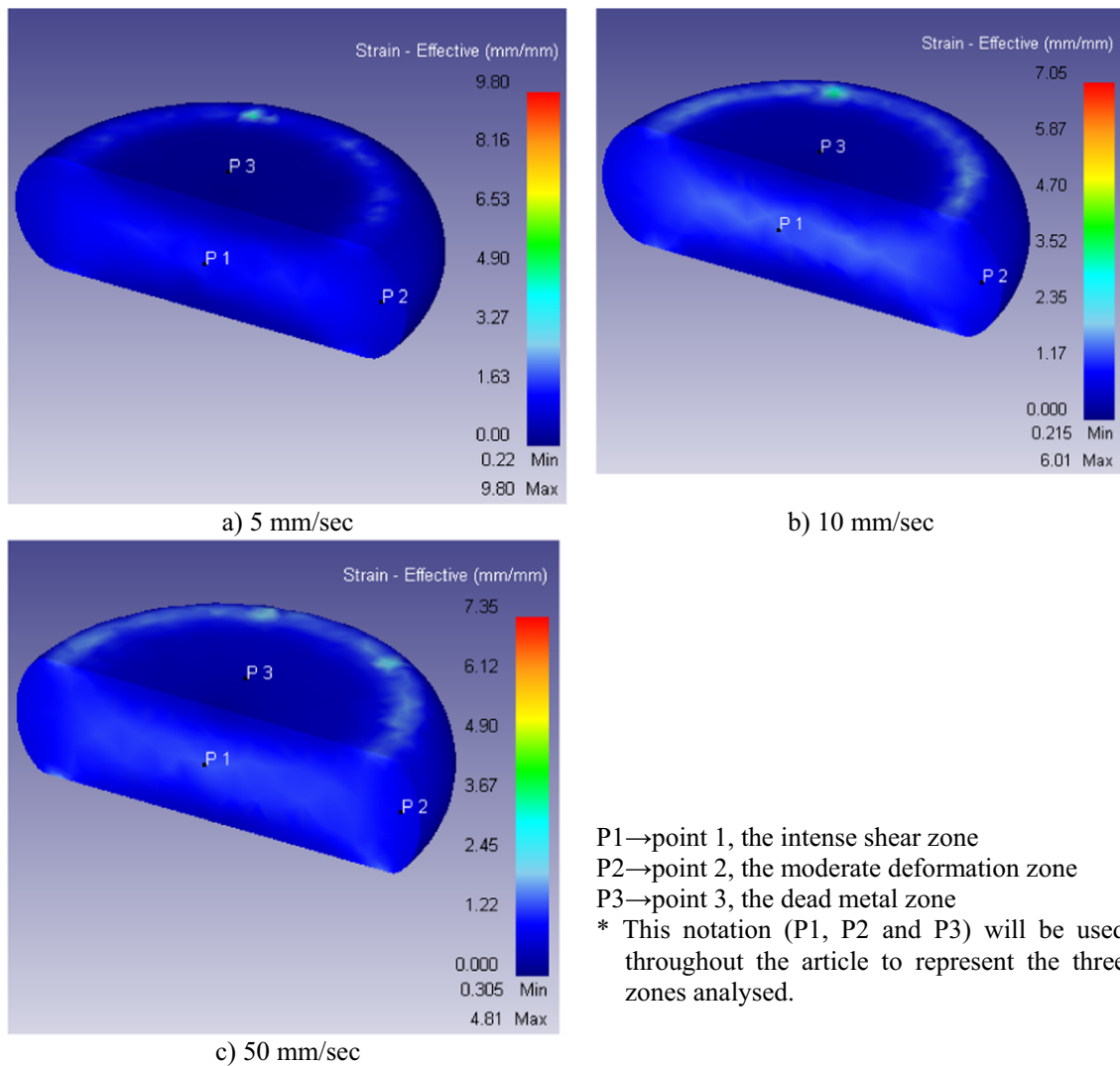


**Fig. 4** Contour map of effective strain distribution at the forming temperature of 1150 °C and different die velocities **a** 5 mm/sec, **b** 10 mm/sec, and **c** 50 mm/sec

The frictional stress acts towards the centre of the workpiece. Thus, this frictional force restricts metal flow during forging. The maximum effective strain (at point P1) values occurred at the centre of the deformed workpiece, as shown in Fig. 5. The maximum strain values obtained from the deformation process were 1.72 (5 mm/sec), 1.57 (10 mm/sec) and 1.54 (50 mm/sec), as shown in Fig. 5. These strain values show that forging at a forming temperature of 1150 °C and die velocity of 5 mm/sec had the highest effective strain. Hence, this strain may cause a more pronounced dynamic recrystallisation. Equbal et al. [29] reported that forging at higher forging temperatures and lower strain rates results in the strain-softening phenomenon. This phenomenon occurs due to long deformation time, causing energy accumulation, boundary mobility and grain recrystallisation growth [11].

### 5.3 Effective stress distribution

Figure 6 shows the effective stress distributions for the entire forging process at a forming temperature of 1150 °C and different die velocities (5, 10, and 50 mm/sec). The deformed sample (Fig. 6) shows an inhomogeneous deformation process during forging. Maximum effective stress occurred at the die-workpiece interface (i.e., point P3). The maximum flow stress values were 196.63 MPa (5 mm/sec), 162.20 MPa (10 mm/sec), and 132.89 MPa (50 mm/sec) under a constant forging simulation temperature of 1150 °C. These flow stress values show that effective flow stress is sensitive to die velocity. The flow behaviour can be affected by friction at the die-workpiece interface, causing high flow stress. Also, the internal heat generation during deformation may cause

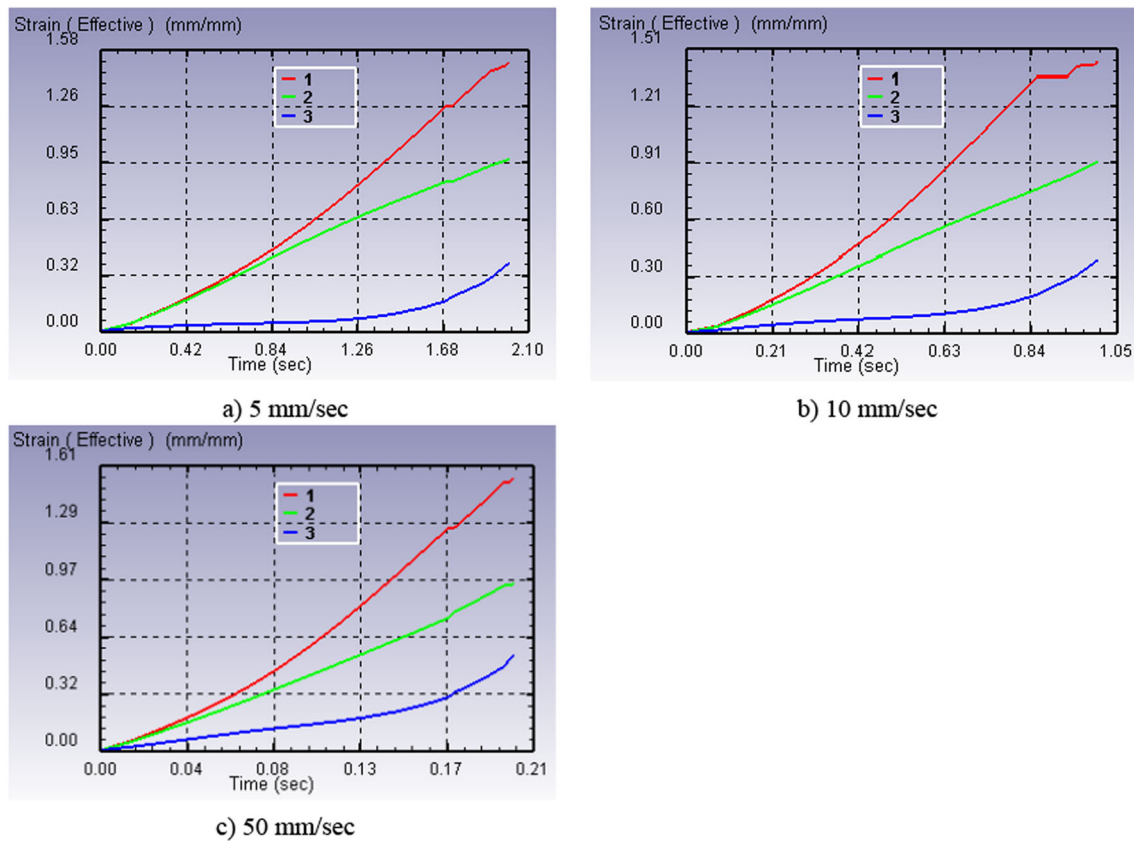


**Fig. 5** Plot of effective strain vs. time showing effective strain distribution of the three points at different die velocities **a** 5 mm/sec, **b** 10 mm/sec, and **c** 50 mm/sec. \* The legend: 1, 2 and 3 represent

points: P1, P2 and P3 respectively. They were obtained using the point tracking technique on the deformed sample

softening, hence reducing flow stress. This variation in deformation behaviour affects measured effective flow stress due to non-isothermal conditions. Thus, the measured flow stress is invalid [17]. To this end, the sole purpose of forming is to break down the carbides and ensure that particles are uniformly distributed in the material, thus improving mechanical properties. Therefore, the variation in temperature, stress, and strain distribution causes an inconsistent forming process, resulting in an uneven grain size refinement process. Hence, uneven grain size affects the overall performance of the component.

Figure 7 shows the variation in the effective flow stress versus the forging time curves for the entire forging simulation at constant forging temperature and different die velocities. The point tracking technique in the software monitored the effective flow stress of three points (P1, P2, and P3). The effective flow stress curves show that at the initial stages of deformation, the flow stress increased rapidly up to 0.14 s (5 mm/sec), 0.07 s (10 mm/sec), and 0.01 s (50 mm/sec), as shown in Fig. 7a–c. At initial deformation, the workpiece exhibited work-hardening characteristics due to an increase in the rate of dislocation density generation [11].

Point P3 had the highest effective flow stress compared to other points (P1 and P2) in all deformation conditions. This higher effective flow stress (point P3) resulted from metal flow restriction and a drop in forging temperature during forging. A sharp temperature drop occurred at the die-workpiece interface due to the chilling effect. The temperature drop at the workpiece/die interface has been reported elsewhere in the literature [7]. The chilling effect occurs due to the temperature gradient between the die and the workpiece, resulting in heat extraction from the workpiece. The chilling effect lowers the workpiece deformation temperature of the pre-set temperature during the forming simulation, resulting in high effective flow stress. At higher deformation, the effective flow stress (points P1, P2, and P3) increased gradually with the deformation time for the entire forging simulation for 5 mm/sec (Fig. 7a) and 10 mm/sec (Fig. 7b) die velocity.

However, a die velocity of 50 mm/sec (Fig. 7c) after the initial deformation (0.01 s) shows different effective flow stress curves for points P1 and P2. The effective flow stress for point P3 increased gradually until the end of the forging simulation, while the effective flow stress of points P1 and P2 reached a maximum flow stress after 0.08 s. P1 and P2 flow stress

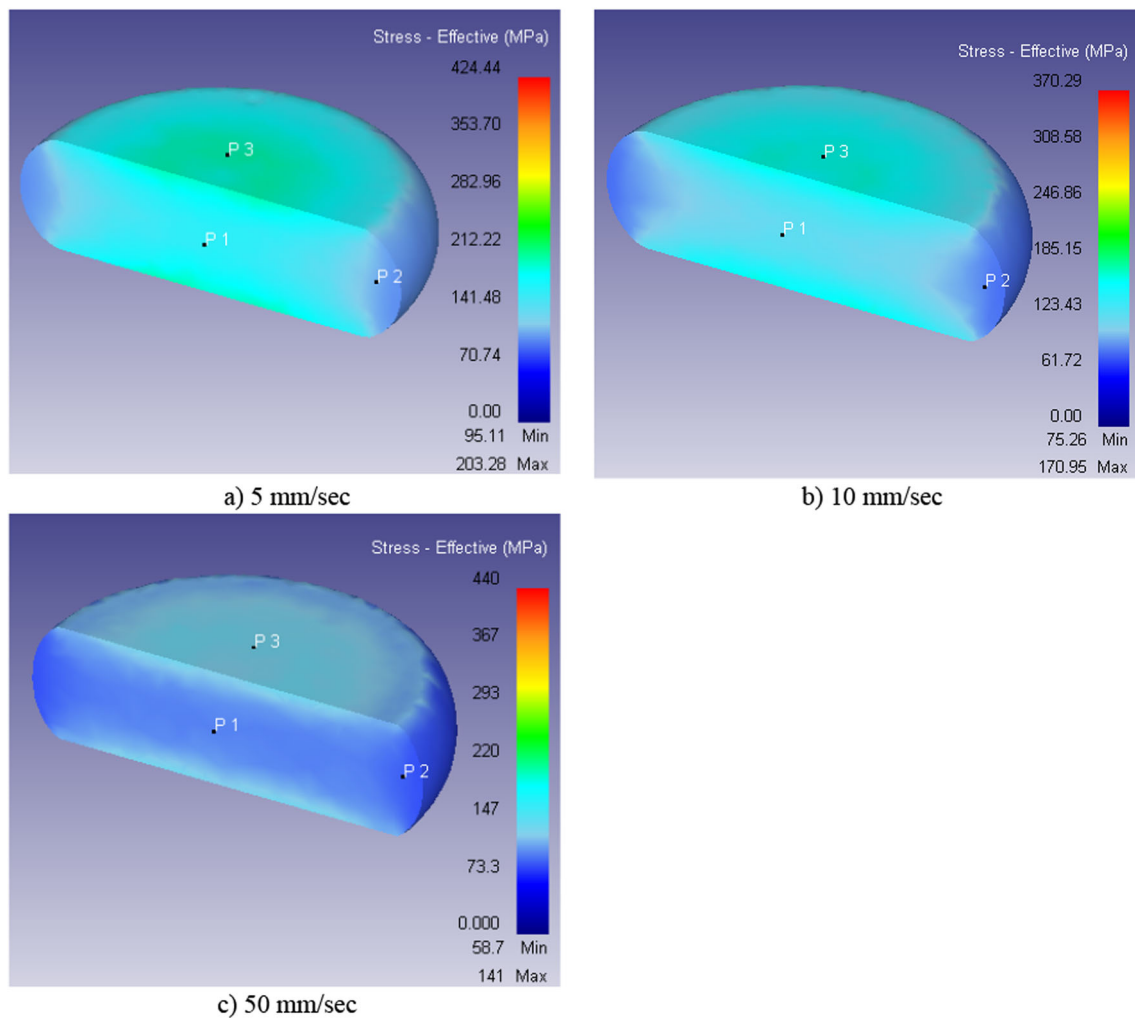


**Fig. 6** Contour map showing effective flow stress distribution at the forming temperature of 1150 °C and different die velocities **a** 5 mm/sec, **b** 10 mm/sec, and **c** 50 mm/sec

curves exhibited a state-steady flow behaviour after 0.08 s up to 0.17 s. After 0.17 s, the flow stress value increased as deformation increased until the end of the simulation process. The higher effective flow stress in higher deformation was due to friction [49].

The study shows that higher stress and strain occur at the centre of the cylinder when forging or upsetting a cylindrical billet. Industrial casting of components results in defect formation, such as pores and voids. These casting defects act as stress concentration sites that can initiate cracks to cause failure. The production route for most industrial components is through castings. Metal forming such as upsetting is used as a secondary process to minimise casting defects, thus improving mechanical properties. Therefore, the high stresses and strains experienced during forging improve the product quality by welding the internal casting defects.

#### 5.4 Particle flow velocity distribution

Figure 8 shows the particle flow velocity distribution at a constant forging temperature and different die velocities during the forging simulation. The 3D simulation plot shows that the particles move towards the nearest surface boundary. The simulation plot shows different colours to denote the velocity magnitude.

The particle flow velocity was maximum, especially at the outer sample surface (red contour) and minimum at the centre of the deformed sample (blue contour), as shown in Fig. 8. The particles on the outer surface of the workpiece flow at a higher flow velocity than on the inner surface. During forging, particle flow velocity mainly depends on the applied compressive force [18].

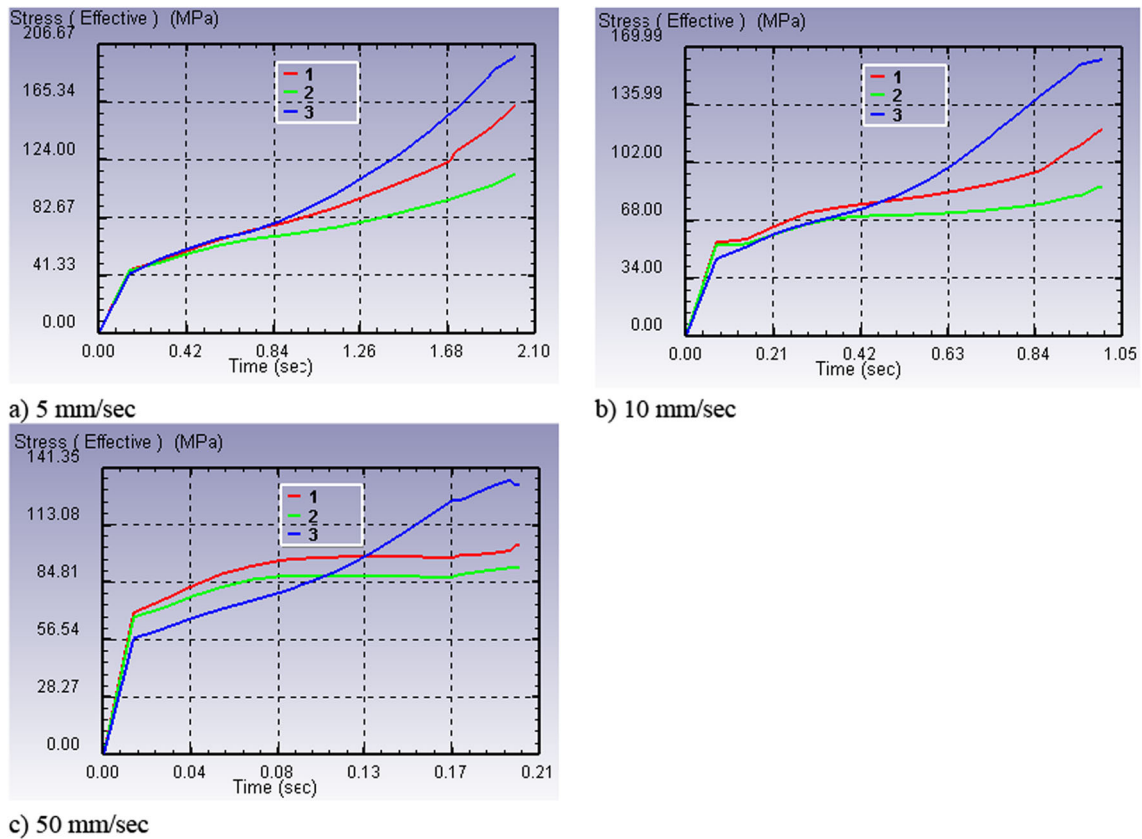


**Fig. 7** Plot of effective stress vs. time showing effective stress distribution of the three points at different die velocities **a** 5 mm/sec, **b** 10 mm/sec, and **c** 50 mm/sec. \* The legend: 1, 2 and 3 represent

points: P1, P2 and P3 respectively. They were obtained using the point tracking technique on deformed the sample

Figure 9 shows the velocity distribution curves at different die velocities and constant temperatures.

Figure 9 shows the particle velocity distribution curves of the three points, P1, P2, and P3. Flow velocity increased rapidly from the beginning of the deformation up to when the forging deformation reached a peak flow velocity in 0.14 s (5 mm/sec), 0.07 s (10 mm/sec), and 0.01 s (10 mm/sec) (

Figure 9). At the initial stage of forming, the material particle experiences high pressure due to high compression forces applied during forging. This pressure makes the particles move quickly to the nearest free surface, as in the case of P3. After the peak flow velocity, P3 maintained a constant particle flow velocity equivalent to the initial die velocity for each deformation case. The steady-state flow velocity may be due to the shear friction stress resisting deformation at the die-workpiece interface.

P1 had the lowest flow velocity compared to the other points in all the deformation conditions. The minimum flow velocity behaviour can be due to the restriction of particle flow at the centre of the cylinder. This flow behaviour indicates that the particles at the centre of the cylinder experience

a lower compressive force, hence less flow movement. Generally, the particle flow velocity for P1, P2, and P3 increased as the die velocity increased at a given constant forming temperature (

Figure 9). Hence, metal flow resistance is less at higher die velocities due to high compressive force.

## 5.5 Strain rate distribution

The effective strain rate distributions for the three points (P1, P2, and P3) in the deformed sample at a constant forging temperature are as in Fig. 10. The results show that point P1 had the highest strain rate compared to the other two points (P2 and P3). A higher strain rate at point P1 indicates that large plastic deformation occurred. Comparing Fig. 5 and Fig. 10, a higher effective strain rate and effective strain occurred at the same point (P1), indicating large plastic deformation. Figure 10 shows that in all die velocities, the effective strain rate increased rapidly with an increase in forging time up to 0.14 s (5 mm/sec), 0.07 s (10 mm/sec), and 0.01 s (50 mm/sec).

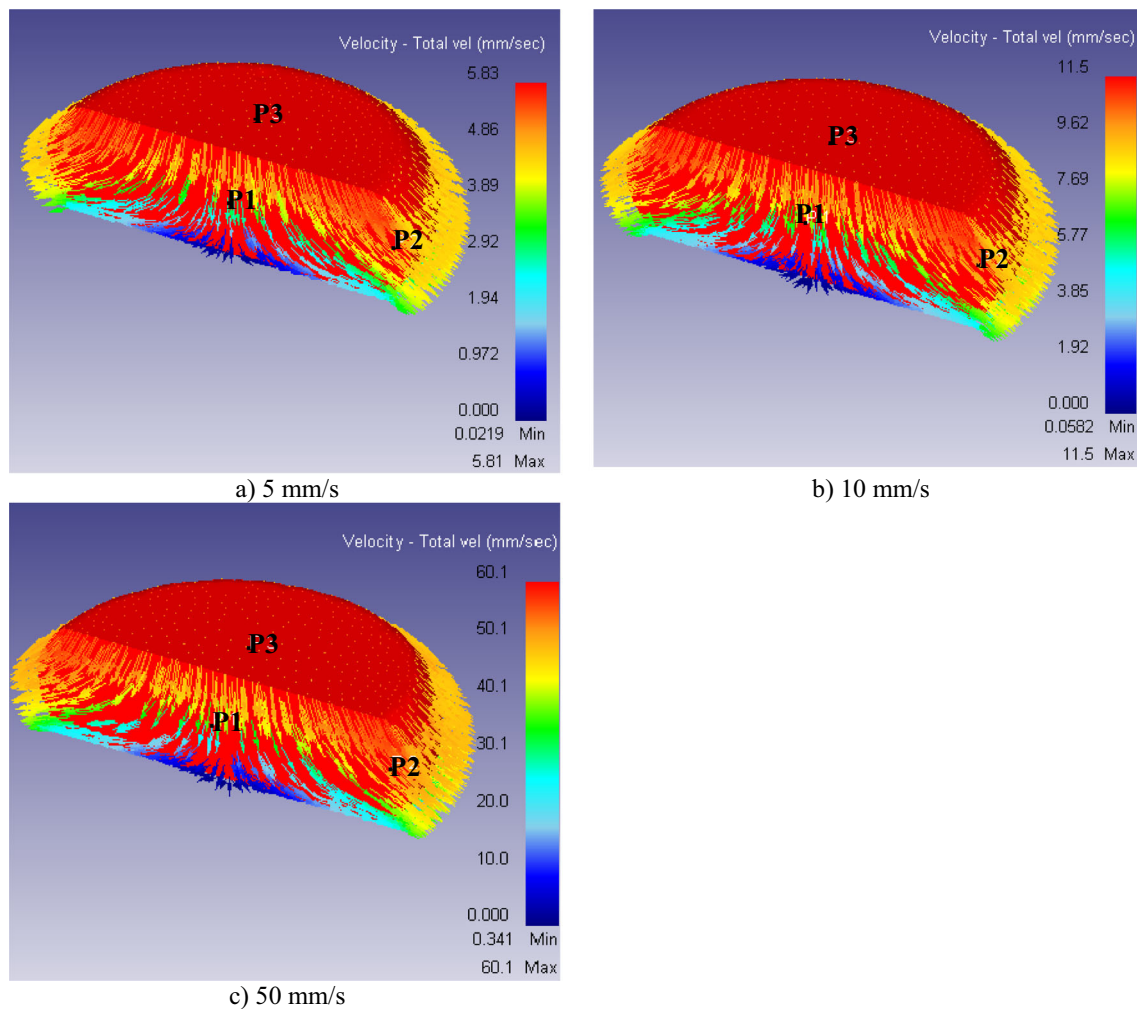


**Fig. 8** Particle flow velocity distribution contour map at forming temperature of 1150 °C and different die velocities **a** 5 mm/sec, **b** 10 mm/sec, and **c** 50 mm/sec

After the initial peak in strain rate, P3 had a strain rate drop for all die velocities and then increased exponentially after 0.84 s (5 mm/sec), 0.42 s (10 mm/sec), and 0.08 s (50 mm/sec) of forging time until the end of the forging simulation. The effective strain rate increased due to increased interfacial friction between the dies and the workpiece. Point P2 maintained a relatively constant strain rate value after an initial rapid increase during the early stages of deformation for all die velocities. The variation in the effective strain rate showed that the forging process was inhomogeneous. From this discussion, it is evident that the strain rate is not constant. However, in most laboratory studies, a constant strain rate value is assumed for all analyses. Therefore, to ensure homogeneous deformation, process parameters optimisation is a must. The process parameter optimisation will enhance the forming process, thus achieving uniform grain size refinement.

## 5.6 Forging temperature distribution

Figure 11 shows the temperature distribution during upsetting at constant temperature and different die velocities. Points P1, P2, and P3, shown in the deformed sample (Fig. 4), have traced the upsetting temperature distribution. The temperature–time curves for die velocities of 5 and 10 mm/sec showed a similar trend of forging temperature drop, Fig. 11a and b.

However, 5 mm/sec forging die velocity had a higher temperature drop than 10 mm/sec. The P3 curve exhibited a similar trend in temperature drop in all forging simulation conditions. The forging temperature drop occurred due to the chilling effect (the heat extraction from the workpiece due to the temperature gradient between the die and the workpiece) at the die-workpiece contact surfaces [7].

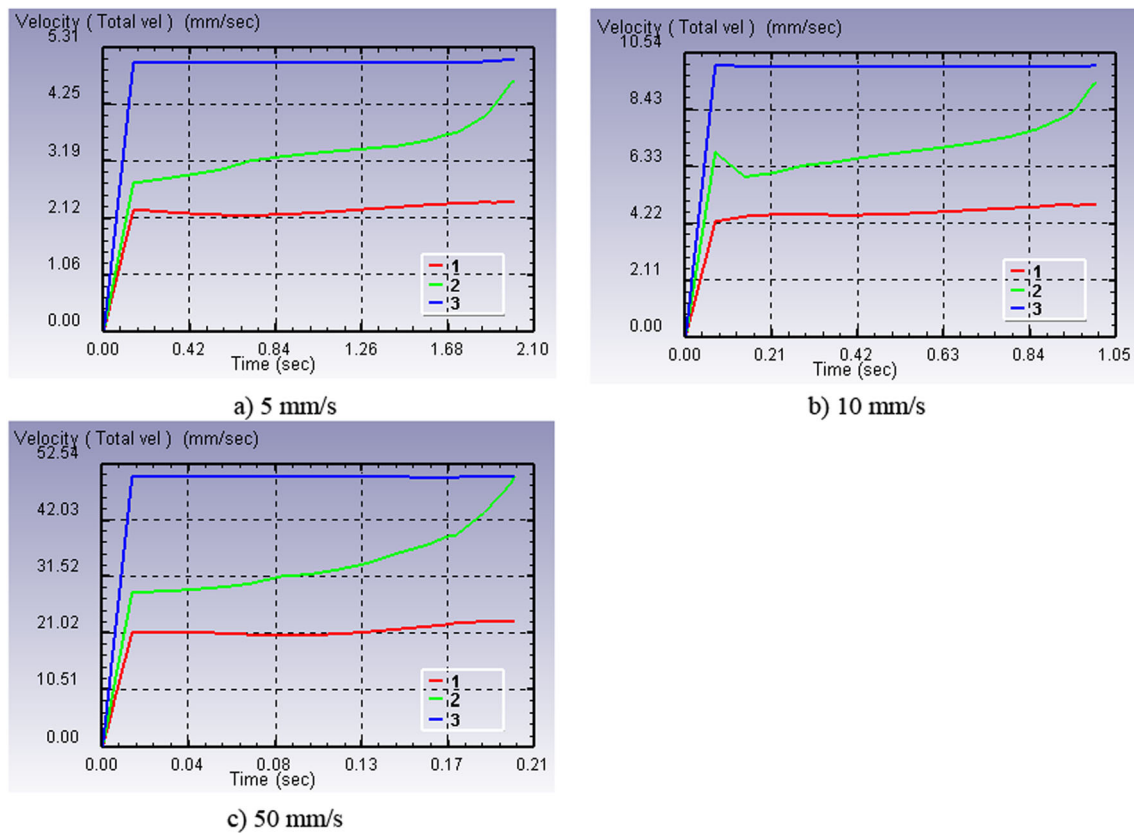


**Fig. 9** A plot of particle velocity vs. time showing particle flow velocity distribution along the forming direction for the three points at a forming temperature of 1150 °C and different die velocities **a** 5 mm/s, **b** 10

mm/sec, and **c** 50 mm/sec. \* The legend: 1, 2 and 3 represent points: P1, P2 and P3 respectively. They were obtained using the point tracking technique on the deformed sample

The temperature difference of the deformed sample causes an inhomogeneous deformation process. P1 and P2 for forging die velocities of 5 and 10 mm/sec had a similar trend in temperature drop but were lower than P3. The reason can be that these two points are not in contact with any surface, thus exchanging heat with the environment. However, P1 and P2 (50 mm/sec) had an increase in forging temperature during forging. This behaviour shows that the two points (P1 and P2) experienced severe plastic deformation, causing internal heat generation. This variation in forging temperature in the deformed sample showed that inhomogeneous deformation occurred during forging, hence a non-isothermal forging process.

## 5.7 Connecting rod FEM simulation

As mentioned, the microstructure and mechanical properties of forged structural and functional components are sensitive to deformation conditions. Therefore, there is a need to provide a further understanding of metal flow patterns during forging. Hence, this information provides a basis necessary

for process optimisation. This section further tries to illustrate the influence of deformation conditions on metal flow patterns during forging. The study used AISI 52100 steel (as before) to simulate an automobile engine connecting rod forging process for conformity.

Figure 12 shows the simulation process setup and the deformed connecting rod sample. The study used the connecting rod model from the inbuilt software geometry. Table 2 gives the simulation conditions. The study illustrates metal flow pattern sensitivity to loading conditions. The results have further confirmed that the metal flow pattern is inhomogeneous during forming, thus affecting microstructure evolution and mechanical properties.

The study considered five tracking points to investigate the metal flow patterns in different areas of the connecting rod ((Fig. 12b). Points P1 (piston pin), P2 (the shank), and P4 (crank pin end) are from the inside of the connecting rod. Points P3 and P5 are on the surface of the crank pin end. Figure 13 shows the metal flow patterns of the connecting rod during forging. The forging temperature, stress, strain, and damage along the tracking points (P1-5) show inhomogeneous deformation behaviour during forging.

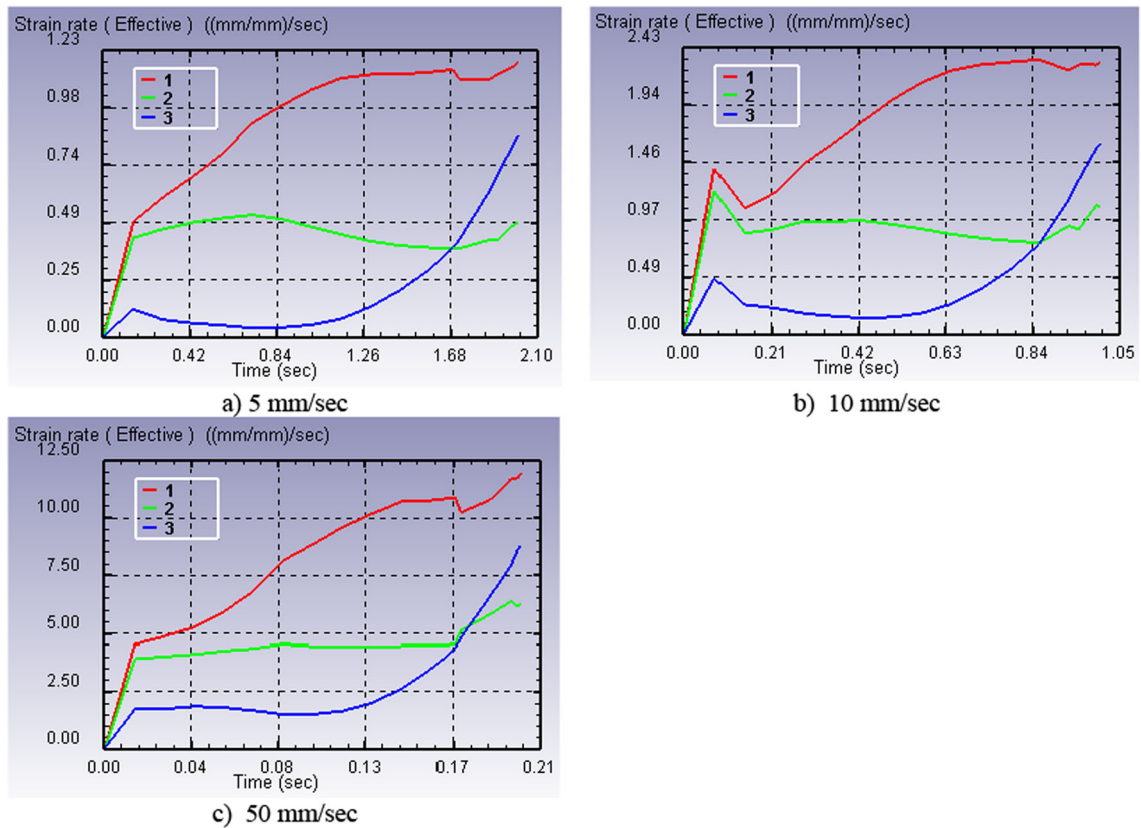


**Fig. 10** A plot of effective strain rate vs. time showing effective strain rate distribution at the three points in the deformed sample at a constant forging temperature of 1150°C. \* The legend: 1, 2 and 3 represent

points: P1, P2 and P3 respectively. They were obtained using the point tracking technique on the deformed sample

For example, Fig. 13a and b shows that the stress and strain distribution varied with the deformation time. All the tracking points indicate different stress and strain values. The variation in stress and strain values can be due to the forging temperature variation during forging (Fig. 13c), thus causing inhomogeneous deformation. Point 4 shows a peculiar temperature drop. This behaviour may be due to a reduction in the cross-section area resulting in close contact between the two dies (top and bottom die). Hence, causing a quicker heat transfer to the environment. This phenomenon accelerates the cooling rate, causing a temperature drop in this region. Generally, during the hot deformation process, plastic deformation causes the generation of internal heat, causing a temperature rise. The damage coefficient (Fig. 13d) indicates the damage probability during forging. A higher damage coefficient indicates a higher damage probability. Generally, P5 showed the highest damage coefficient (0.2), which means that damage is most likely to occur at this point of the connecting rod during forging. The study has shown that metal flow behaviour during upsetting (forging) is inhomogeneous, resulting in inferior mechanical properties due to varied microstructure variation. Therefore, process

parameter optimisation is paramount to determine the optimal processing conditions for high product quality during industrial metal forming processes.

## 6 Industrial implications and future directions

The forging process has been in existence dating back to the Industrial Revolution for the manufacture of hand tools and other equipment. Forging or upsetting finds application in producing most machine parts. As such, the incorporation of the finite element method (FEM) in the production process has optimised the production parameters [24]. The FEM has been in existence for more than 40 years ago. The 3D FEM approach has revolutionised the industrial manufacturing processes such as forging. High-processing computers have enabled the development of finite element software codes. These software codes enhanced the production process by studying and optimising the metal flow behaviour [24, 48].

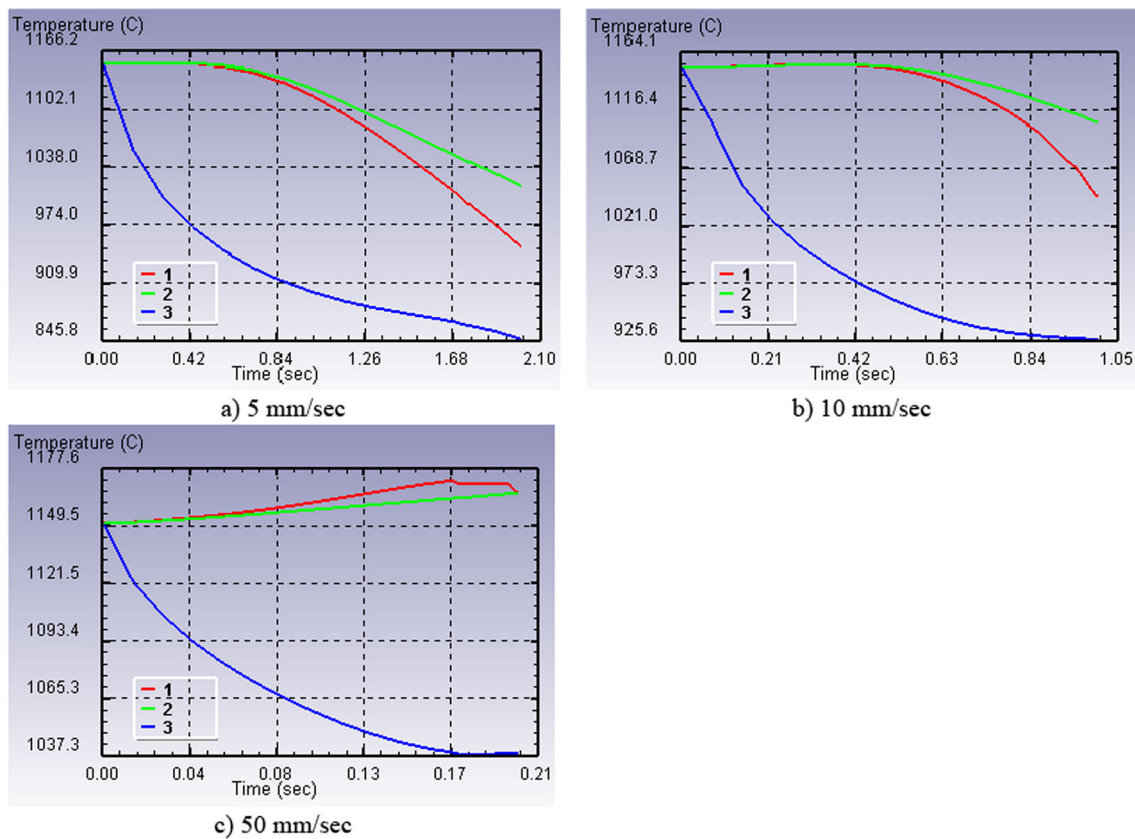


**Fig. 11** Plot of deformation vs. time showing temperature distribution at the three points in the deformed sample. \* The legend: 1, 2 and 3 represent points: P1, P2 and P3 respectively. They were obtained using the point tracking technique on the deformed sample

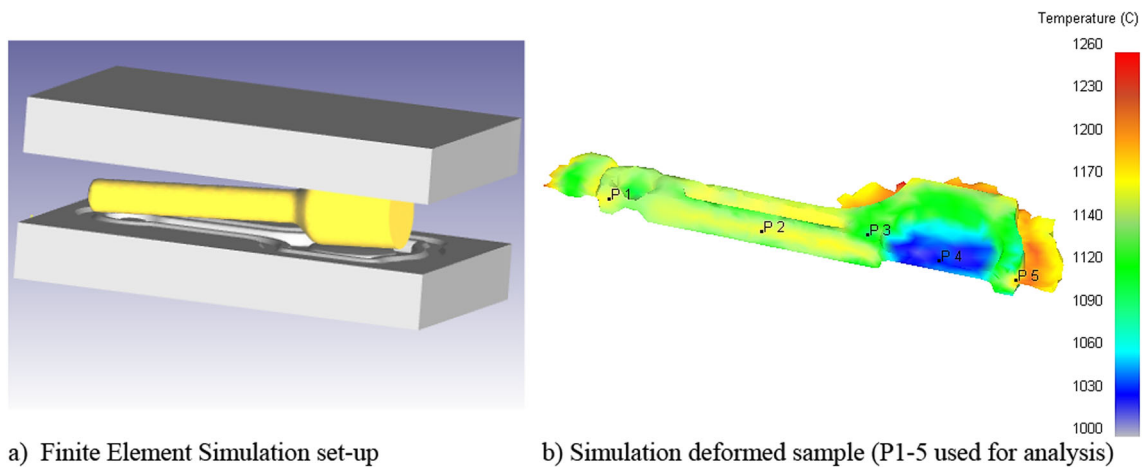


**Fig. 12** Forging simulation process

Researchers have widely used the FEM tool to predict and accurately describe real-life problems such as the metal deformation process [2]. However, the application of FEM still faces challenges. The challenge is to achieve accuracy in FEM computational analysis. The FEM simulation results depend on the understanding of the material properties and behaviour, process parameters, geometry description and the

boundary conditions [50]. These factors need attention during the design of the simulation process. Statistical tools and Dynamic Material modelling (DMM) are widely applied in process parameter optimisation [51, 52]. Studies on metal flow behaviour and forging parameters optimisation are readily available in the literature. Therefore, future research should focus on the die tool design and life [50]. Progress is

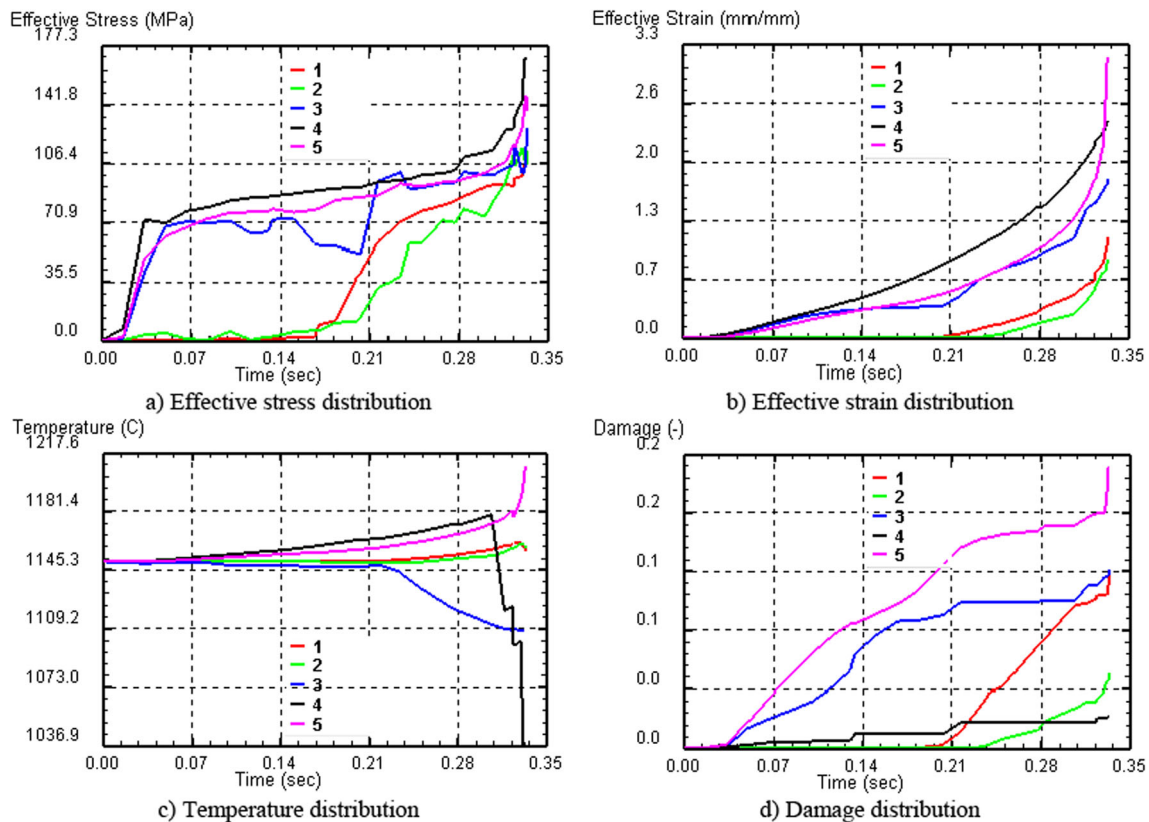


**Fig. 13** Plots illustrating metal flow behaviour due to deformation conditions (forging temperature of 1150°C and die speed 50 mm/sec) (\*Legend key: 1,2,3,4 and 5 represent Points 1–5 on the deformed workpiece in Fig. 12b)

ongoing to improve tool life and design, study stress distribution, and reduce tool wear. Future development also requires a fully developed production chain that can study and predict microstructure during metal forming. Therefore, the computational tool needs an enhancement towards achieving high processing capacity to reduce the computational time.

## 7 Conclusions

The forging simulation of AISI 52100 high-chromium steel was studied using the finite element method. From the simulation results, the following are the conclusions:

1. The forging load-time curves showed that the forging load increased with a decrease in the forging temperature at a constant die velocity. Under constant forging temperature, the 5 mm/sec die velocity had a higher forging load. This behaviour can be due to friction change from dynamic to static, causing deformation resistance. The results show that deformation was inhomogeneous due to variations in stress/strain distribution across the deformed sample. The maximum effective strain occurred at the centre of the deformed sample.

This temperature drop was due to the temperature gradient at the die-sample contact surfaces. The temperature variation during forging causes inhomogeneous flow behaviour variation across the sample.

2. The particle flow velocity curves showed a similar flow trend for all tested conditions. The particle flow velocity increased as die velocity increased at a constant forging temperature. The flow velocity increase suggests a lower resistance to deformation at higher die velocities. Lower particle flow velocity occurred at the inner centre surface of the deformed sample due to flow restriction and lower compressive forces.
3. Forging simulation of an engine connecting rod further confirms that inhomogeneous deformation occurs during upsetting (forging). The deformation conditions affect flow behaviour, causing variations in microstructure evolution during forging. The microstructure variation affects the overall mechanical performance of the component. Therefore, process optimisation is paramount.
4. From the FEM results, the analysis and optimisation of most industrial metal forming processes by using numerical simulation methods is possible. The results show the effectiveness and efficiency of using FEM as a routine

tool for designing and optimising the metal forming processes.

**Funding** Open access funding provided by Tshwane University of Technology.

**Data Availability** The data used to support the findings of this study are included within the article.

## Declarations

**Conflicts of interest** The authors declare that they have no conflicts of interest regarding the publication.

**Open Access** This article is licensed under a Creative Commons Attribution 4.0 International License, which permits use, sharing, adaptation, distribution and reproduction in any medium or format, as long as you give appropriate credit to the original author(s) and the source, provide a link to the Creative Commons licence, and indicate if changes were made. The images or other third party material in this article are included in the article's Creative Commons licence, unless indicated otherwise in a credit line to the material. If material is not included in the article's Creative Commons licence and your intended use is not permitted by statutory regulation or exceeds the permitted use, you will need to obtain permission directly from the copyright holder. To view a copy of this licence, visit <http://creativecommons.org/licenses/by/4.0/>.

## References

- Ohdar, R.K., Equbal, A., Equbal, M.I.: Hot deformation studies of AISI 1035 steel using thermo mechanical simulator. *Mater. Today Proc.* **26**, 3305–3310 (2020). <https://doi.org/10.1016/j.matpr.2020.02.469>
- Maarefdoust, M.: Simulation of finite volume of hot forging process of industrial gear. *Int. Proc. Comput. Sci. Inf. Technol.* **57**, 111–115 (2012). <https://doi.org/10.1063/1.3623660>
- Rajamuthamilselan, M., Ramanathan, S.: Hot deformation behaviour of 7075 alloy. *J. Alloys Compd.* **509**(3), 948–952 (2011). <https://doi.org/10.1016/j.jallcom.2010.09.139>
- D. George, *Mechanical Metallurgy McGraw-Hill Book Company, New York*. 1988.
- Beddoes, J., Bibby, M.J.: Principles of metal manufacturing processes. Oxford UK (1999). <https://doi.org/10.1016/B978-034073162-8/50012-6>
- Zhang, Z.J., Dai, G.Z., Wu, S.N., Dong, L.X., Liu, L.L.: Simulation of 42CrMo steel billet upsetting and its defects analyses during forming process based on the software DEFORM-3D. *Mater. Sci. Eng. A* **499**(1–2), 49–52 (2009). <https://doi.org/10.1016/j.msea.2007.11.135>
- Rasti, J., Najafzadeh, A., Meratian, M.: Correcting the stress-strain curve in hot compression test using finite element analysis and Taguchi method. *Int. J. ISSI* **8**(1), 26–33 (2011)
- Oh, S.I.: Finite element analysis of metal forming processes with arbitrarily shaped dies. *Int. J. Mech. Sci.* **24**(8), 479–493 (1982). [https://doi.org/10.1016/0020-7403\(82\)90058-3](https://doi.org/10.1016/0020-7403(82)90058-3)
- Chen, F., Ren, F., Cui, Z., Lai, X.: Constitutive modeling for elevated temperature flow behavior of 30Cr2Ni4MoV ultra-supercritical rotor steel. *J. Iron. Steel Res. Int.* **21**(5), 521–526 (2014). [https://doi.org/10.1016/S1006-706X\(14\)60081-9](https://doi.org/10.1016/S1006-706X(14)60081-9)
- Lin, Y.C., Chen, M.S., Zhong, J.: Prediction of 42CrMo steel flow stress at high temperature and strain rate. *Mech. Res. Commun.* **35**(3), 142–150 (2008). <https://doi.org/10.1016/j.mechrescom.2007.10.002>
- Zhu, L., He, J., Zhang, Y.: A two-stage constitutive model of X12CrMoWVNbN10-1-1 steel during elevated temperature. *Mater. Res. Express* **5**, 026505 (2018). <https://doi.org/10.1088/2053-1591/aaa911>
- Li, L., Zhou, J., Duszczyc, J.: Determination of a constitutive relationship for AZ31B magnesium alloy and validation through comparison between simulated and real extrusion. *J. Mater. Process. Technol.* **172**(3), 372–380 (2006). <https://doi.org/10.1016/j.jmatprotec.2005.09.021>
- Christiansen, P., Martins, P.A.F., Bay, N.: Friction compensation in the upsetting of cylindrical test specimens. *Exp. Mech.* **56**(7), 1271–1279 (2016). <https://doi.org/10.1007/s11340-016-0164-z>
- Gao, P.F., Guo, J., Zhan, M., Lei, Z.N., Fu, M.W.: Microstructure and damage based constitutive modelling of hot deformation of titanium alloys. *J. Alloys Compd.* (2020). <https://doi.org/10.1016/j.jallcom.2020.154851>
- Samantaray, D., Mandal, S., Bhaduri, A.K.: Optimization of hot working parameters for thermo-mechanical processing of modified 9Cr-1Mo (P91) steel employing dynamic materials model. *Mater. Sci. Eng. A* **528**(15), 5204–5211 (2011). <https://doi.org/10.1016/j.msea.2011.03.025>
- Liu, X.G., Ji, H.P., Guo, H., Jin, M., Guo, B.F., Gao, L.: Study on hot deformation behaviour of 316LN austenitic stainless steel based on hot processing map. *Mater. Sci. Technol.* **29**(1), 24–29 (2013). <https://doi.org/10.1179/1743284712Y.0000000083>
- Evans, R.W., Scharning, P.J.: Axisymmetric compression test and hot working properties of alloys. *Mater. Sci. Technol.* **17**(8), 995–1004 (2001). <https://doi.org/10.1179/026708301101510843>
- Obiko, J.O., Mwema, F.M., Bodunrin, M.O.: Finite element simulation of X20CrMoV121 steel billet forging process using the Deform 3D software. *SN Appl. Sci.* (2019). <https://doi.org/10.1007/s42452-019-1087-y>
- Mwema, F.M., Obiko, J.O., Akinlabi, E.T., Akinlabi, S.A., Fatoba, O.S.: Effect of punch force on the upsetting deformation process using three-dimensional finite element analysis. *J. Phys. Conf. Ser.* (2019). <https://doi.org/10.1088/1742-6596/1378/3/032094>
- Gholamzadeh, A., Karimi Taheri, A.: The prediction of hot flow behavior of Al-6%Mg alloy. *Mech. Res. Commun.* **36**(2), 252–259 (2009). <https://doi.org/10.1016/j.mechrescom.2008.06.011>
- Mostafaei, M.A., Kazeminezhad, M.: The prediction of hot flow behavior of Al-6%Mg alloy. *Mater. Sci. Eng. A* **535**, 216–221 (2012). <https://doi.org/10.1016/j.msea.2011.12.067>
- Luan, J., Sun, C., Li, X., Zhang, Q.: Constitutive model for AZ31 magnesium alloy based on isothermal compression test. *Mater. Sci. Technol.* **30**(2), 211–219 (2014). <https://doi.org/10.1179/1743284713Y.0000000341>
- Hu, M., Dong, L., Zhang, Z., Lei, X., Yang, R., Sha, Y.: Correction of flow curves and constitutive modelling of a Ti-6AL-4V alloy. *Metals (Basel)* **8**(4), 256 (2018). <https://doi.org/10.3390/met8040256>
- Oh, S.I., Wu, W.T., Tang, J.P., Vedhanayagam, A.: Capabilities and applications of FEM code deform: the perspective of the developer. *J. Mater. Process. Tech.* **27**(1–3), 25–42 (1991). [https://doi.org/10.1016/0924-0136\(91\)90042-D](https://doi.org/10.1016/0924-0136(91)90042-D)
- Murillo-Marrodán, A., Puchi-Cabrera, E., García, E., Dubar, M., Cortés, F., Dubar, L.: An incremental physically-based model of P91 steel flow behaviour for the numerical analysis of hot-working processes. *Metals (Basel)* **8**(4), 269 (2018). <https://doi.org/10.3390/met8040269>
- Kumar, P., Panda, S.S.: Numerical simulation of Al1070 alloy through hybrid SPD process. *Int. J. Adv. Manuf. Technol.* **91**(1–4), 835–846 (2017). <https://doi.org/10.1007/s00170-016-9768-9>

27. Wei, Z., Yandong, Y.: High-temperature rheological behavior and numerical simulation technology for 6061 aluminum alloy connecting rods. *J. Eng. Sci. Technol. Rev.* **11**(6), 116–124 (2018). <https://doi.org/10.25103/jestr.116.15>
28. Cai, Z., Ji, H., Pei, W., Wang, B., Huang, X., Li, Y.: Constitutive equation and model validation for 33Cr23Ni8Mn3N heat-resistant steel during hot compression. *Results Phys.* **15**, 102633 (2019). <https://doi.org/10.1016/j.rinp.2019.102633>
29. Equbal, M.I., Talukdar, P., Kumar, V., Ohdar, R.K.: Deformation Behavior of Micro-alloyed Steel by Using Thermo Mechanical Simulator and Finite Element Method. *Procedia Mater. Sci.* **6**, 674–681 (2014). <https://doi.org/10.1016/j.mspro.2014.07.083>
30. Wang, S., Huang, Y., Xiao, Z., Liu, Y., Liu, H.: A modified Johnson-Cook model for hot deformation behavior of 35CrMo steel. *Metals (Basel)* **7**(9), 337 (2017). <https://doi.org/10.3390/met7090337>
31. Samantaray, D., Mandal, S., Bhaduri, A.K.: Constitutive analysis to predict high-temperature flow stress in modified 9Cr-1Mo (P91) steel. *Mater. Des.* **31**(2), 981–984 (2010). <https://doi.org/10.1016/j.matdes.2009.08.012>
32. Lin, Y.C., Chen, M.S., Zhang, J.: Modeling of flow stress of 42CrMo steel under hot compression. *Mater. Sci. Eng. A* **499**(1–2), 88–92 (2009). <https://doi.org/10.1016/j.msea.2007.11.119>
33. Yin, F., Hua, L., Mao, H., Han, X.: Constitutive modeling for flow behavior of GCr15 steel under hot compression experiments. *Mater. Des.* **43**, 393–401 (2013). <https://doi.org/10.1016/j.matdes.2012.07.009>
34. Lin, Y.C., Chen, X.M.: A critical review of experimental results and constitutive descriptions for metals and alloys in hot working. *Mater. Des.* **32**(4), 1733–1759 (2011). <https://doi.org/10.1016/j.matdes.2010.11.048>
35. He, A., Xie, G., Yang, X., Wang, X., Zhang, H.: A physically-based constitutive model for a nitrogen alloyed ultralow carbon stainless steel. *Comput. Mater. Sci.* **98**, 64–69 (2015). <https://doi.org/10.1016/j.commatsci.2014.10.044>
36. He, A., Xie, G., Zhang, H., Wang, X.: A comparative study on Johnson-Cook, modified Johnson-Cook and Arrhenius-type constitutive models to predict the high temperature flow stress in 20CrMo alloy steel. *Mater. Des.* **52**, 677–685 (2013). <https://doi.org/10.1016/j.matdes.2013.06.010>
37. Zhang, P., Yi, C., Chen, G., Qin, H., Wang, C.: Constitutive model based on dynamic recrystallization behavior during thermal deformation of a nickel-based superalloy. *Metals (Basel)* **6**(7), 161 (2016). <https://doi.org/10.3390/met6070161>
38. Jha, J.S., Tewari, A., Mishra, S., Toppo, S.: Constitutive relations for Ti-6Al-4V hot working. *Procedia Eng.* **173**, 755–762 (2017). <https://doi.org/10.1016/j.proeng.2016.12.089>
39. Ji, H., Cai, Z., Pei, W., Huang, X., Lu, Y.: DRX behavior and microstructure evolution of 33Cr23Ni8Mn3N: experiment and finite element simulation. *J. Mater. Res. Technol.* **9**(3), 4340–4355 (2020). <https://doi.org/10.1016/j.jmrt.2020.02.059>
40. Lv, C., Zhang, L., Mu, Z., Tai, Q., Zheng, Q.: 3D FEM simulation of the multi-stage forging process of a gas turbine compressor blade. *J. Mater. Process. Technol.* **198**(1–3), 463–470 (2008). <https://doi.org/10.1016/j.jmatprotec.2007.07.032>
41. Kukuryk, M.: Analysis of deformation and damage evolution in hot elongation forging. *Arch. Metall. Mater.* **57**(2), 417–424 (2012). <https://doi.org/10.2478/v10172-012-0041-4>
42. Kukuryk, M.: Numerical analysis of strains and stresses in the hot cogging process. *J. Appl. Math. Comput. Mech.* **17**(3), 45–52 (2018). <https://doi.org/10.17512/jamcm.2018.3.04>
43. Asadi, P., Mahdavinejad, R.A., Tutunchilar, S.: Simulation and experimental investigation of FSP of AZ91 magnesium alloy. *Mater. Sci. Eng. A* **528**(21), 6469–6477 (2011). <https://doi.org/10.1016/j.msea.2011.05.035>
44. Chakraborty, M., Banerjee, N., De, S.: Analysis and optimization of die geometry for forging dies in railway wheel manufacturing. *Int. J. Interact. Des. Manuf.* **18**(4), 2449–2465 (2023). <https://doi.org/10.1007/s12008-023-01508-0>
45. Anoop, A.D., Sekhar, A.S., Kamaraj, M., Gopinath, K.: Modelling the mechanical behaviour of heat-treated AISI 52100 bearing steel with retained austenite. *J. Mater. Des. Appl.* (2015). <https://doi.org/10.1177/1464420715612235>
46. Mwema, F.M., Obiko, J.O., Mahamood, R.M., Adedirin, A.A., Michael Bodunrin, E.T., Akinlabi, T.C.J.: Constitutive analysis of hot forming process of P91 steel: finite element method approach. *Adv. Mater. Process. Technol.* **8**(sup3), 1182–1193 (2022). <https://doi.org/10.1080/2374068X.2021.1939560>
47. Bodunrin, M., Obiko, J., Klenam, D.: On the uniaxial compression testing of metallic alloys at high strain rates: an assessment of DEFORM-3D simulation. *Appl. Sci.* (2023). <https://doi.org/10.3390/app13042686>
48. Ketabchi, M., Mohammadi, H., Izadi, M.: Finite-element simulation and experimental investigation of isothermal backward extrusion of 7075 Al alloy. *Arab. J. Sci. Eng.* **37**(8), 2287–2296 (2012). <https://doi.org/10.1007/s13369-012-0320-4>
49. Li, Y.P., Onodera, E., Matsumoto, H., Chiba, A.: Correcting the stress-strain curve in hot compression process to high strain level. *Metall. Mater. Trans. A* **40**(4), 982–990 (2009). <https://doi.org/10.1007/s11661-009-9783-7>
50. Andrietti, S., Chenot, J.L., Bernacki, M., Bouchard, P.O., Fourment, L., Hachem, E., Perchat, E.: Recent and future developments in finite element metal forming simulation. *Comput. Methods Mater. Sci.* **15**(2), 265–293 (2015)
51. Oirere, J., Fredrick, O., Mwema, M., Shangwira, H.: Forging optimisation process using numerical simulation and Taguchi method. *SN Appl. Sci.* (2020). <https://doi.org/10.1007/s42452-020-2547-0>
52. Mohapatra, S.K., Maity, K.P.: Parametric optimization of simulated extrusion of square to square section through linear converging die. *IOP Conf. Ser. Mater. Sci. Eng.* (2016). <https://doi.org/10.1088/1757-899X/115/1/012031>

**Publisher's Note** Springer Nature remains neutral with regard to jurisdictional claims in published maps and institutional affiliations.